Article

Modeling critical thermoelectric transports driven by band broadening and phonon softening

Kunpeng Zhao [1,2,5] ✉, Zhongmou Yue[1,3,5], Hexige Wuliji[2], Hongyi Chen [4] ✉, Tingting Deng[1,3], Jingdan Lei [2], Pengfei Qiu [1,3], Lidong Chen [1,3] & Xun Shi [1,3] ✉

Critical phenomena are one of the most captivating areas of modern physics, whereas the relevant experimental and theoretical studies are still very challenging. Particularly, the underlying mechanism behind the anomalous thermoelectric properties during critical phase transitions remains elusive, i.e., the current theoretical models for critical electrical transports are either qualitative or solely focused on a specific transport parameter. Herein, we develop a quantitative theory to model the electrical transports during critical phase transitions by incorporating both the band broadening effect and carrier-soft TO phonon interactions. It is found that the band-broadening effect contributes an additional term to Seebeck coefficient, while the carrier−soft TO phonon interactions greatly affects both electrical resistivity and Seebeck coefficient. The universality and validity of our model are well confirmed by experimental data. Furthermore, the features of critical phase transitions are effectively tuned. For example, alloying S in Cu_2Se can reduce the phase transition temperature but increase the phase transition parameter b. The maximum thermoelectric figure of merit zT is pushed to a high value of 1.3 at the critical point (377 K), which is at least twice as large as those of normal static phases. This work not only provides a clear picture of the critical electrical transports but also presents new guidelines for future studies in this exciting area.

Critical phenomena are common in nature[1,2], such as the increase in compressibility upon approaching the critical point of liquid-vapor equilibrium[3], the increase in magnetic susceptibility and dielectric constant in the vicinity of the Curie points of ferromagnets and feorroelectrics[4], the anomaly in heat capacity at the point of critical transition[5], and the abnormally thermoelectric (TE) properties at the point of critical phase transition[6–13]. Particularly, the materials

undergoing critical phase transitions have pronounced atomic disorder and critical fluctuations (Fig. 1a), which bring about a rich diversity of electrical and thermal transports near the critical point[6–19]. For instance, anomalous reduction in thermal conductivity κ has been observed during critical phase transitions for a lot of materials, such as Cu_2Se[6,15] and $BaTiO_3$[20]. Dramatic increment in ρ have been reported around the ferroelectric phase transitions of $SnTe$[16,21], $PbTe$[22], $GeTe$[8],

[1]State Key Laboratory of High Performance Ceramics and Superfine Microstructure, Shanghai Institute of Ceramics, Chinese Academy of Sciences, Shanghai 200050, China. [2]State Key Laboratory of Metal Matrix Composites, School of Materials Science and Engineering, Shanghai Jiao Tong University, Shanghai 200240, China. [3]Center of Materials Science and Optoelectronics Engineering, University of Chinese Academy of Sciences, 100049 Beijing, China. [4]College of Chemistry and Chemical Engineering, Central South University, Changsha, Hunan 410083, China. [5]These authors contributed equally: Kunpeng Zhao, Zhongmou Yue. ✉e-mail: zkp.1989@sjtu.edu.cn; hongyichen@csu.edu.cn; xshi@mail.sic.ac.cn
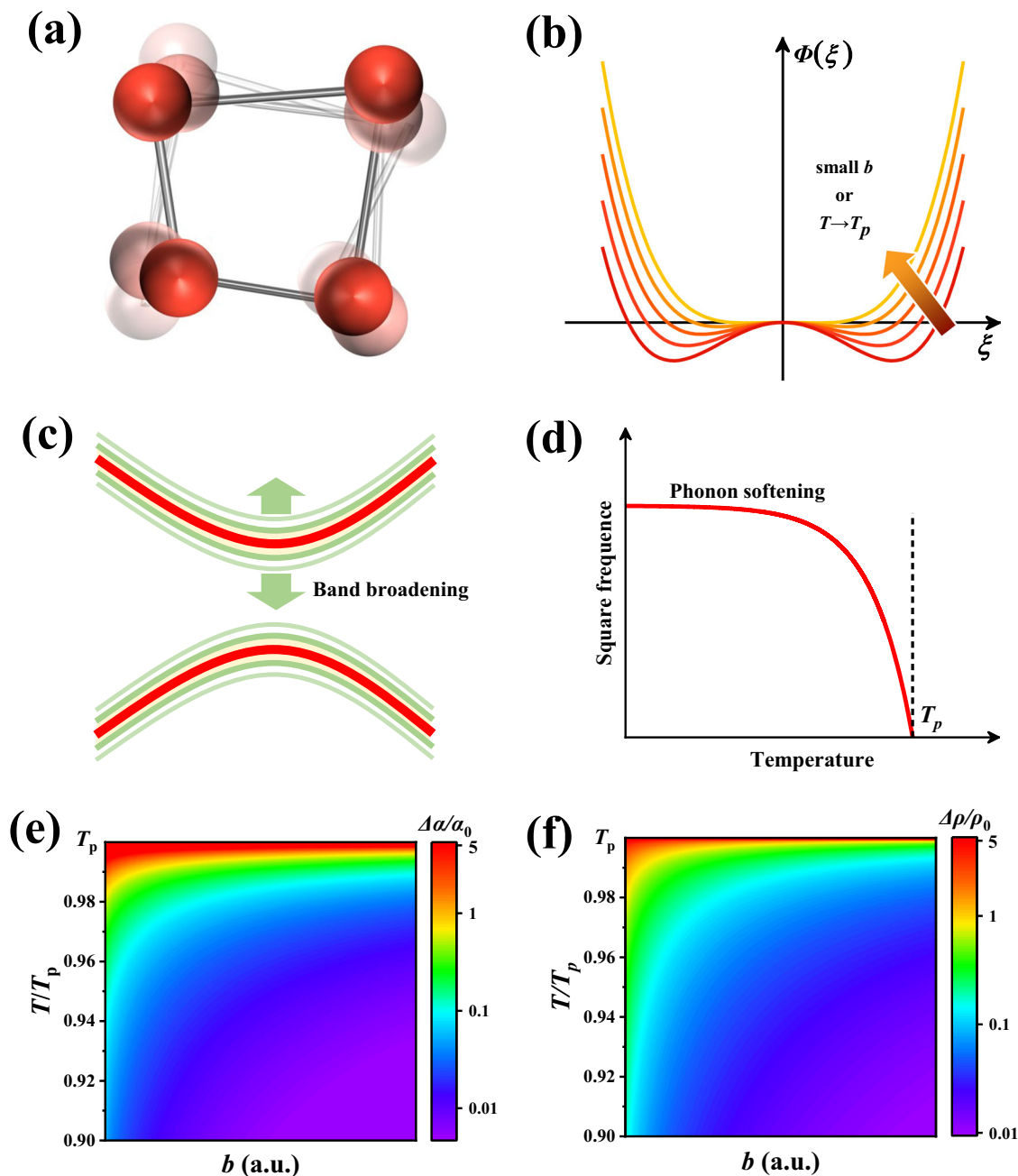
Fig. 1 | Band broadening and phonon softening by structural fluctuation during critical second-order phase transitions. a Schematic map of structural fluctuation, (**b**) Free energy Φ as a function of order parameter ξ for different b or temperatures. Schematic maps of (**c**) band broadening and (**d**) phonon softening effects. **e** Illustration of the relatively enhanced Seebeck coefficient ($\Delta\alpha/\alpha_0$) driven by band broadening and phonon softening effects (red indicating large $\Delta\alpha/\alpha_0$ and purple indicating small $\Delta\alpha/\alpha_0$, as shown in the scale on the right), with respect to the temperature (T) and phase transition parameter b. **f** The relatively enhanced electrical resistivity ($\Delta\rho/\rho_0$) attributed by carrier-soft TO phonon interaction, with respect to the temperature (T) and phase transition parameter b.

and their ternary alloys. Likewise, sharp enlargements in both ρ and α were observed in the vicinity of phase transition of Cu_2Se[6,15,18,23–25]. Combining these effects, abnormally enhanced TE figure of merit ($zT = \alpha^2 T/\rho\kappa$) with the λ shape during critical phase transitions is obtained, alike the other critical physical properties during phase transitions. The mechanisms for the critical TE transports have been also studied recently, such as the strong critical scattering[6,15], soft transverse-optical (TO) modes[26–30], the increased structure entropy[17,18], broad energy gap[31], and gradually changed electronic states[32]. However, in most cases, these models are typically qualitative or just consider specific mechanisms. Furthermore, many of them only solely focus on either the electrical resistivity or the Seebeck coefficient,

rather than the whole electrical transports. A quantitative and comprehensive model covering both electrical conductivity and Seebeck coefficient during critical phase transitions is still absent until today, which greatly restricts the understanding of the physics involved and hampers the discovery of new critical TE materials.

In this work, starting from the Landau theory, we developed a theoretical model to quantitatively describe both electrical resistivity and Seebeck coefficient during critical phase transitions by incorporating the band broadening effect and carrier-soft TO phonon interactions. Subsequently, this model is successfully validated by experimental data and serves as a useful guide for designing novel TE materials with critical transports.

Results and discussion

Modeling of the critical electrical transports

A second-order phase transition is generally critical, which refers to the continuous structural transition from a low-temperature ordered phase to a high-temperature disordered phase accompanied by continuous change of entropy and volume[33–35]. The order parameter ξ, a measure of the character and strength of the broken symmetry, was proposed by Landau to describe the order-disorder transition (see details in the Supplementary Information)[35]. Generally, ξ has a zero value above the transition temperature and a nonzero value below the transition temperature. When temperature approaches the critical phase transition point T_p, the ξ fluctuates in a range of $\xi_0(T) \pm \Delta\xi$, where the distribution of $\Delta\xi$ follows the Maxwell-Boltzmann distribution[35]

$$w(\Delta\xi) = A_\xi e^{-\frac{\Delta\Phi}{k_B T}} \tag{1}$$

Here A_ξ is a normalized constant, k_B is the Boltzmann constant, T is the absolute temperature, and $\Delta\Phi$ is the energy required for the fluctuation of ξ, which is approximate to $\Delta\Phi \approx 2b \times (T - T_p) \times (\Delta\xi)^2$ for a small departure from the equilibrium state. As shown in Fig. 1b, fewer energy is required for the fluctuation of ξ when phase transition parameter b is small or temperature is close to T_p.

The variation of ξ implies the critical fluctuations in atoms site, lattice strain, and crystal symmetry (Fig. 1a), which would lead to two important effects. One is the broadening or smearing of band-edge density of states[7,36] (Fig. 1c), and the other is the softening of transverse-optic (TO) phonons[37,38] (Fig. 1d). Here we try to quantitatively give the formula how these effects influence the electrical resistivity and Seebeck coefficient. Based on the classical Landau theory[33,35], the distribution function of the band energy E is given by

$$w(E) = A_\xi e^{-\frac{(E-E_0)^2}{\Delta^2}} \tag{2}$$

where Δ is a broadening function and given by

$$\Delta = \left(\frac{k_B c^2 T}{2b(T_p - T)}\right)^{\frac{1}{2}} \tag{3}$$

Here c is the first derivate of energy with respect to order parameter. The derived Gaussian distribution of band broadening and the temperature dependency of broadening function Δ are well consistent with the band-smearing effect in RbAg4I5 reported by Bauer et al.[36] A small b value or a temperature close to T_p obviously lead to a large broadening of band-edge energy. Mahan[31] presented a theory for the anomalous critical Seebeck coefficient based on a fitted Δ from experimental data. After substitution of Δ (i.e. Eq. (3)) into Mahan's derivation, the formulas for the material with band broadening is obtained

$$\frac{\Delta\alpha_1}{\alpha_0} = \frac{3c^2}{8\pi^2 b} \frac{1}{T T_p (1 - T/T_p)^2} \tag{4}$$

$$\rho = \frac{3}{2e^2} \frac{1}{\Sigma(\eta)} \tag{5}$$

where α_0 is the normal Seebeck coefficient of a conductor[39], and $\Delta\alpha_1$ is the enhanced Seebeck coefficient from band broadening. $\Sigma(\eta) = \int \frac{d^3k}{(2\pi)^3} v_k^2 \tau(k) \delta(k)$, where v_k is the electronic wave factor, and τ_k is the relaxation time of electrons. Clearly, the band broadening effect during critical phase transitions has no impact on electrical resistivity, but contributes an additional term to Seebeck coefficient. The enhanced $\Delta\alpha_1$ strongly depends on the temperature T and phase

transition parameter b. At the critical point T_p, the maximum ratio $\frac{\Delta\alpha_{1,max}}{\alpha_0}$ approaches infinity, which, however, is unable to be determined in experiments because the Seebeck coefficient is measured within a certain temperature difference range. Below T_p, $\frac{\Delta\alpha_1}{\alpha_0}$ is inversely proportional to b, i.e. a smaller b would yield a larger Seebeck coefficient.

Now we turn to study the effect of softening of transverse-optic (TO) phonons on critical electrical transports. Based on the standard theory of the second-order phase transition, the soft TO phonon frequency ω decreases rapidly when T is approaching to T_p (Fig. 1d)[40]

$$\omega^2 = b(T_p - T) \tag{6}$$

The enhanced electrical resistivity $\Delta\rho_2$ caused by phonon softening (see the derivation details in the Supplementary Information) is then given by

$$\frac{\Delta\rho_2}{\rho_0} = C_1 T \left[1 - \frac{b(T_C - T)}{\gamma} \ln\left(1 + \frac{\gamma}{b(T_C - T)}\right)\right] \tag{7}$$

Here $C_1 = \frac{\sqrt{2}}{16} \frac{k_B}{MD} \left|\frac{V_p}{a}\right|^2 \frac{m^{\frac{1}{2}} \tau_0 E_F^{-\frac{1}{2}+s}}{\hbar^2}$, which is a parameter independent on temperature T and phase transition parameter b, V_p is the potential energy of electron-phonon interaction, and γ is related to the dispersion coefficient D and Fermi vector of electrons k_F, which is given by $\gamma = 4Dk_F^2$[28]. s represents the scattering factor and takes the value of -0.5 for acoustic phonon scattering and 0.5 for optical phonon scattering. When T is approaching to T_p or b is reduced, $\Delta\rho_2$ is significantly enhanced due to the strong interaction between carriers and soft TO phonons, as illustrated in Fig. 1f. At the critical point T_p, the maximum ratio $(\frac{\Delta\rho_{max}}{\rho_0} = C_1 T_p)$ is obtained, which is independent on parameter b. This is understandable because the TO phonon frequency ω becomes zero at the critical point irrespective of b (see Eq. 6).

Furthermly, the impact of phonon softening on Seebeck coefficient can be determined by solving the Mott expression (see the derivation details in the Supplementary Information):

$$\frac{\Delta\alpha_2}{\alpha_0} = \frac{\Delta\rho_2/\rho_0}{1 + \Delta\rho_2/\rho_0} \frac{\frac{1}{2} - s}{s + \frac{3}{2}} \tag{8}$$

where $\Delta\alpha_2$ is the additional Seebeck coefficient contributed by the phonon softening. It is clear that $\Delta\alpha_2$ arises from the change of scattering mechanism. If the electrical conduction of the normal phase is dominated by the optical phonon scattering (i.e. $s = 0.5$), $\Delta\alpha_2$ becomes zero due to the fact that phase transition-induced electrical transport is also governed by optical phonon scattering.

Incorporating the band broadening and phonon softening effects, the enhanced Seebeck coefficient $\Delta\alpha$ during critical phase transition is given by:

$$\frac{\Delta\alpha}{\alpha_0} = \frac{3c^2}{8\pi^2 b} \frac{1}{T T_p (1 - T/T_p)^2} + \frac{\Delta\rho_2/\rho_0}{1 + \Delta\rho_2/\rho_0} \frac{\frac{1}{2} - s}{\frac{3}{2} + s} \tag{9}$$

Equations (7) and (9) are the quantitively relationship for critical electrical transports (α and ρ), which are strongly correlated via parameter b. As the temperature approaches T_p or b is reduced, the fluctuation of order parameter ξ becomes critical, leading to much increased Seebeck coefficient and electrical resistivity, as illustrated in Figs. 1e and 1f.

It should be noted that there are certain approximations or biases in the modeling. Firstly, we only considered the second power of the order parameter ξ while neglected the fourth and higher power of ξ, which has a little impact on the electrical transports when the temperature is very close to the critical point. Secondly, we applied Taylor series expansion to the band-edge energy E near ξ_0 based on the Landau theory rather than the quantum theory. Thirdly, the relationship between the Fermi wave vector k_F and the Fermi energy E_F was
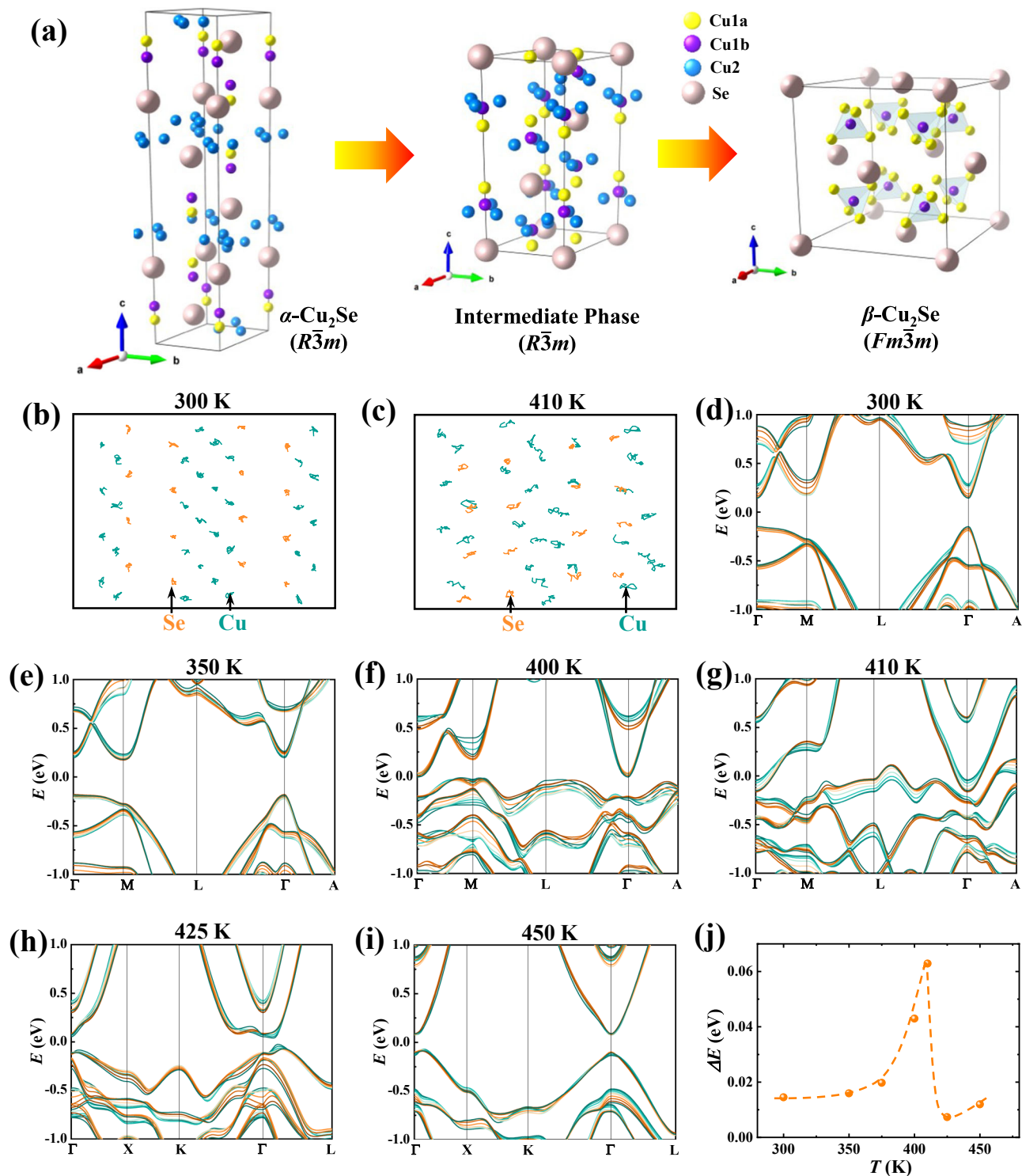
Fig. 2 | Evolution of crystal structure and band structure during critical phase transitions for Cu2Se. a Crystal structures of the low temperature trigonal phase, intermediate phase, and high temperature cubic phase. Atomic trajectories derived from molecular dynamics simulations at (**b**) 300 K and (**c**) 410 K. The Cu and Se atoms are colored by cyan and yellow, respectively. Calculated band structures at (**d**) 300 K, (**e**) 350 K, (**f**) 400 K, (**g**) 410 K, (**h**) 425 K, and (**i**) 450 K. **j** The broadened energy ΔE of the valence band edge as a function of temperature.

derived using the single parabolic band model. The expressions of electrical resistivity ρ_0 and Seebeck coefficient α_0 for the normal phases were also derived under the assumption of relaxation time approximation and single parabolic band of degenerate semiconductors. These approximations or assumptions may introduce certain biases or oversights between theory and experiment.

Universality and verification of the model

The well-known liquid-like TE material Cu2Se with critical phase transition is selected to verify our model. The phase transition of Cu2Se is completely reversible except for slight hysteresis during cooling (Supplementary Fig. 1a). At room temperature, Cu2Se adopts a layered trigonal structure ($R\bar{3}m$)[41] with all atoms orderly distributed
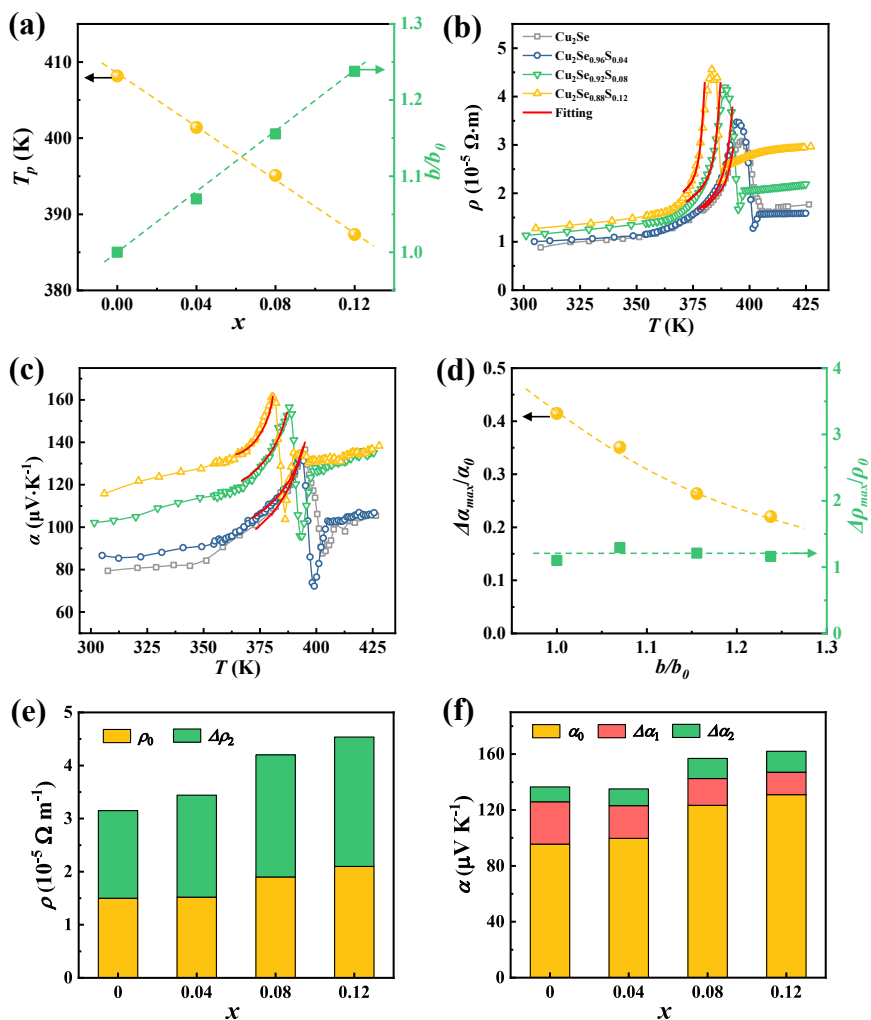
Fig. 3 | Tuning the critical electrical transports during phase transitions in Cu$_2$Se$_{1-x}$S$_x$. a Critical temperature T_p and the relative phase transition parameter b/b_0 as a function of S content x. b_0 denotes the phase transition parameter for Cu$_2$Se. Temperature dependence of (**b**) electrical resistivity ρ and (**c**) Seebeck coefficient α. Red lines represent the fitting results by our model. **d** The maximum relative increment of electrical resistivity $\Delta\rho_{max}/\rho_0$ and Seebeck coefficient $\Delta\alpha_{max}/\alpha_0$ at T_p as a function of phase transition parameter b/b_0. The dashed lines are guide to the eyes. The respective contribution of (**e**) electrical resistivity and (**f**) Seebeck coefficient from the normal phase (ρ_0 and α_0), the band broadening effect ($\Delta\alpha_1$), and the carrier-soft TO phonon interactions ($\Delta\rho_2$ and $\Delta\alpha_2$) at the critical point.

in the crystal lattice. Upon heating, part of Cu migrates from the copper rich to the copper deficient layer, ultimately transforming into a disordered cubic structure ($Fm\bar{3}m$)[42] above the critical temperature (T_p ~ 410 K, see Fig. 2a). Accordingly, the order parameter goes continuously from finite value to zero at T_p. Ab initio molecular dynamics (MD) simulations and band structure calculations were performed to understand the structural fluctuation and band broadening effect. As shown in Fig. 2b, all atoms vibrate in the vicinity of their equilibrium positions at 300 K, whereas part of Cu atoms migrate toward the copper deficient layer and interact with Se from the adjacent neighboring layer at 410 K (Fig. 2c). Compared to the atomic trajectories at 300 K, both Cu and Se vibrate in a much larger space at 410 K, implying the crystal structure is undergoing a critical fluctuation near the critical temperature T_p. The valence band edge shows a clear broadening as T approaches T_p. Specifically, the broadened energy ΔE is only 0.014 eV at 300 K, but it is sharply increased to 0.063 eV at 410 K and finally drops to 0.007 eV at 425 K (Fig. 2i). The λ-shaped ΔE implies that the band broadening is caused by structural fluctuations, not thermal vibrations. Besides, the band gap E_g is obviously decreased as the temperature increases, which is probably caused by the enhanced interaction between Se and Cu.

The broadened band edge and decreased E_g near T_p well attest to the band broadening effect during critical phase transitions.

Step-wise increase trends in ρ and α are observed in the normal trigonal and cubic phases of Cu$_2$Se. However, during the phase transition region, the ρ sharply increases by a factor of 2.9 while α sharply increases by a factor of 1.4 when the temperature approaches to T_p. The obtained power factor ($PF = \alpha^2/\rho$) exhibits a trench-like shape near the critical point (Supplementary Fig. 2a). The sharp increasement of ρ and α are obviously contributed by the carrier−soft transverse-optical (TO) phonon interaction and band broadening effect. Using the derived Eqs. (7) and (9), we fitted the critical electrical properties near T_p with the fitting parameters shown in Table S1. Here the b value is taken as 1.5×10^{26} for both ρ and α. A good agreement between the experimental data (symbols in Fig. 3b, c) and theoretical estimation (red lines) is obtained in the phase transition region. This implies that our model is universal and can link all the critical electrical transports through parameter b. Furthermore, the fitted T_p is 413 K, consistent well with the experimental data (409.5 K) determined from the measurement of C_p. And the fitted γ value is on the order of 10^{25} s^{-2}, which is also comparable to the value of 7.6×10^{25} s^{-2} estimated from the neutron measurement[37,43]. All these results well support and verify our models.
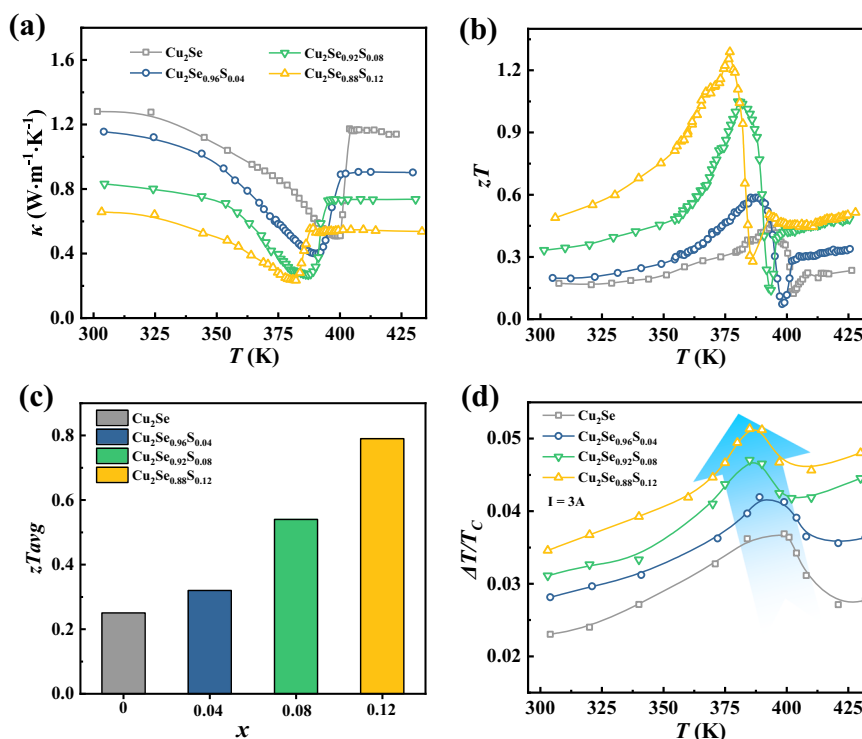
Fig. 4 | Thermal conductivity, TE figure of merit zT, and cooling performance. Temperature dependence of (**a**) thermal conductivity κ and (**b**) zT values for $Cu_2Se_{1-x}S_x$ ($x = 0$, 0.04, 0.08 and 0.12). **c** Average zT from 300 K to the critical point.

d $\Delta T/T_C$ *vs* temperature measured at $I = 3$ A for the TE unicouple made of p-type $Cu_2Se_{1-x}S_x$ and n-type $Yb_{0.3}Co_4Sb_{12}$. T_C is the temperature of the cold junction side. Solid lines are guides to the eyes.

Tuning of the critical thermoelectric properties

Since the critical electrical transports during phase transitions are directly affected by parameter b and phase transition temperature, we try to alloy the analogous element S at Se sites in Cu_2Se to tune the features of critical phase transitions. The single trigonal phase with homogenously distributed elements is observed (see XRD and EDS results in Supplementary Fig. 3) in $Cu_2Se_{1-x}S_x$ solid solutions, with the phase transition features greatly altered. The critical temperature (T_p) is gradually reduced when increasing the content of S (Supplementary Figs. 1b, 3a), which is mainly attributed to the less energy difference between the low-temperature phase and high-temperature phase, i.e. the smaller enthalpy change (ΔH, Table S2) during phase transition for S-alloyed Cu_2Se compared to pristine Cu_2Se. Similar phenomenon has been observed in a lot of solid solutions, such as $Cu_7PSe_{6-x}Te_x$[44] and $Cu_{2-x}Ag_xTe$[45]. Meanwhile, the phase transition region is gradually narrowed after the substitution of S at Se sites. According to the Landau theory, the specific heat (C_p) near critical point is in direct proportion to the square of phase transition parameter, i.e. $C_p \propto b^2$ (see details in the Supplementary Information)[35]. Therefore, the relative phase transition parameter b/b_0 for $Cu_2Se_{1-x}S_x$ can be readily derived from the slope of tangent lines near T_p (see dashed lines in Supplementary Fig. 1b). Clearly, when increasing S content, b is gradually improved (Fig. 3a). Specifically, the b value for $x = 0.12$ is 1.24 times of that in Cu_2Se.

Alloying S at the Se sites can increase the bonding energy to fix Cu atoms in the crystal lattice[46], which successfully suppresses the formation of Cu vacancies and gives rise to the reduced hole concentrations (i.e., the improved Fermi level). As a result, both electrical resistivity ρ and Seebeck coefficient α are greatly improved with increasing S content. Similar to the temperature dependency of Cu_2Se, step-wise increase in the normal phases and sharp increase during phase transitions are observed for ρ and α in $Cu_2Se_{1-x}S_x$. Alloying S shifts the peak values to lower temperature, being in accordance with the DSC results. Likewise, we fitted the abnormal electrical properties

near T_p using Eqs. (7) and (9). The derived b values gradually increase with increasing S content, which aligns with our experimental results. The parameter C_1 gradually decreases while γ gradually increases with an increase of S content, which is also reasonable since C_1 is in an inverse relation to the Fermi level while γ is positively correlated with the Fermi level. Figure 3d exhibits the maximum increment of electrical resistivity $\Delta\rho_{max}/\rho_0$ and Seebeck coefficient $\Delta\alpha_{max}/\alpha_0$ at T_p as a function of b/b_0. When increasing b/b_0, the $\Delta\rho_{max}/\rho_0$ is nearly unchanged but $\Delta\alpha_{max}/\alpha_0$ is gradually decreased, which are also fully consistent with our theoretical prediction. Based on the fitting results of our model, we can also derive the respective contributions from the band broadening effect ($\Delta\alpha_1$) and the carrier-soft TO phonon interactions ($\Delta\rho_2$ and $\Delta\alpha_2$). As shown in Figs. 3e and 3f, the enhanced resistivity $\Delta\rho_2$ is gradually increased owing to the increased Fermi level. Meanwhile, the enhanced Seebeck coefficient $\Delta\alpha_1$ during the critical phase transition is reduced whereas $\Delta\alpha_2$ is slightly improved because the former is largely impacted by the parameter b while the latter is primarily determined by the scattering mechanism. Overall, alloying S in Cu_2Se proves to be an effective way to tune the strength of band broadening effect and carrier-soft TO phonon interactions.

The critical fluctuation during phase transitions also has a large impact on thermal transports. A sharp, cusp-like dip near the critical point is observed in κ for $Cu_2Se_{1-x}S_x$ (Fig. 4a). The minimal κ is only 0.24 W m⁻¹ K⁻¹ near T_p for $Cu_2Se_{0.08}S_{0.12}$, which is only one third of that in normal phases. The lattice thermal conductivity κ_L shows the similar dip trend with κ, and the κ_L value approaches zero at the critical point (Supplementary Fig. 2c). The anomalous reduction in κ_L during phase transitions is majorly attributed to the strong coupling of heat-carrying acoustic phonons with soft optic phonons[20]. Figure 4b shows the temperature dependence of figure of merit zT for $Cu_2Se_{1-x}S_x$. Owing to the significantly enhanced α and decreased κ, the zT values are greatly improved during phase transitions. A maximum zT of 1.3 is achieved at 377 K for $Cu_2Se_{0.88}S_{0.12}$, which is at least 1.5 times larger than those of normal trigonal and cubic phases, and represents a 190% improvement

over that of Cu_2Se. Moreover, the average zT from 300 K to the critical point is also as high as 0.8 (Fig. 4c), which is also among the top values of TE materials. Such remarkable TE performance near room temperature makes it highly competitive with the state-of-the-art TE materials like Bi_2Te_3[47] and Mg_3Bi_2[48].

To further confirm the significantly improved zT values during phase transitions, we constructed a series of unicouples consisting of p-type $Cu_2Se_{1-x}S_x$ and n-type $Yb_{0.3}Co_4Sb_{12}$ TE materials with the cooling performance shown in Supplementary Fig. 4 (see details in the Experimental Section). When the direct current is applied, the temperature at cold junction (T_C) is dramatically reduced due to the Peltier effect. When increasing current, the temperature drop (ΔT) is gradually increased and eventually saturated at around 12 A (Supplementary Fig. 4). The maximum temperature difference (ΔT) values achieved in the phase transition region are higher than those of normal trigonal and cubic phases. Figure 4d shows the values of $\Delta T/T_C$ at different temperatures under a small current of 3 A. Obviously, the temperature dependent $\Delta T/T_C$ shows a similar λ shape as that of zT values. $\Delta T/T_C$ is greatly improved during phase transitions with a maximum enhancement of more than 48% as compared with the trigonal and cubic phases. In addition, the maximum $\Delta T/T_C$ is shifted to lower temperatures when increasing S content.

In summary, previous theoretical models for critical electrical transports were either qualitative or solely focused on a specific mechanism. Herein, we propose a quantitative model covering both electrical conductivity and Seebeck coefficient to explain the critical properties during phase transitions by including the band broadening effect and carrier-soft TO phonon interactions. This model is well validated by the experiment data in Cu_2Se and has been successfully used to explore and tune the critical features of S alloyed Cu_2Se. Considering the universal behavior often exhibited by critical phenomena, whereby the same underlying mathematical and physical principles apply across various systems, we believe our findings can not only offer valuable insights for future studies on critical thermoelectric transports but also provide inspiration for the exploration of other complex systems such as magnets, fluids, and biological systems. For example, the heat capacity anomaly at the critical transition is also caused by the fluctuations in the order parameter of the system, similar to the electrical properties in our model. At temperatures below the critical point, the order parameter is nonzero and the system is ordered. As the temperature approaches the critical point, the fluctuations in the order parameter become more pronounced and the system becomes more disordered. Therefore, theoretically, it is also possible to derive a model for heat capacity based on the Landau theory. Experimentally, the abnormal heat capacity during critical transitions have been observed in various systems, such as ferromagnetic UGe_2[5], liquid crystals[49], and $Pb_{1-x}Ge_xTe$ alloys[50]. This strongly suggests that the critical phenomena and its physical models are universal. It is worth noting that the narrow temperature range of phase transitions restricts its practical applications. Future studies should focus more on the tuning and broadening of phase transition temperature range. For example, we can alloy or dope the material with appropriate elements to reduce the energy difference between the low-temperature and high-temperature phases. Besides, by fabricating a functionally graded material with a multilayer structure, we can potentially harness the critical properties of different compositions and thus extend the temperature range of phase transition.

Methods
Materials synthesis
Polycrystalline $Cu_2Se_{1-x}S_x$ ($x = 0$, 0.04, 0.08 and 0.12) and $Yb_{0.3}Co_4Sb_{12}$ were prepared from high purity elements: Cu (shots, 99.999%, Alfa Aesar), Se (shots, 99.999%, Alfa Aesar), S (pieces, 99.999%, Alfa Aesar), Co (shots, 99.99%, Alfa Aesar), Sb (shots, 99.999%, Alfa Aesar) and Yb (ingots, 99.95%, Alfa Aesar). The required elements were weighted out

in the pyrolytic nitride crucible according to the nominal chemical compositions. The crucible was enclosed in fused silica tube under vacuum. Then, the tubes were heated up to 1423 K in 12 h and kept at this temperature for 12 h, and then cooled to 923 K over 50 h. After being annealed at 923 K for 6 days, the tubes were cooled to ambient temperature naturally. Only a few cooper whiskers were observed on the surface of Cu_2Se, which were removed after annealing. Subsequently, the ingots were grounded into fine powder and sintered by a spark plasma sintering facility (SPS, Sumitomo SPS-2040) at 723 K for 10 min under a pressure of 65 MPa. Thermally conducting and electrically insulating BN layers were sprayed onto the inner surface of carbon dies and carbon foils to prevent the Cu migration during sintering process. The raw materials for $Yb_{0.3}Co_4Sb_{12}$ were sealed in the evacuated silica tubes, melted at 1353 K, and then quenched to room temperature, followed by annealing at 923 K for over 6 days. The grounded powder was sintered by SPS at 873 K under a pressure of 60 MPa. The relative density of all samples was above 98%.

Thermoelectric unicouple fabrication
A series of thermoelectric unicouples based on p-type $Cu_2Se_{1-x}S_x$ and n-type $Yb_{0.3}Co_4Sb_{12}$ was constructed and tested. Firstly, p-type $Cu_2Se_{1-x}S_x$ and n-type $Yb_{0.3}Co_4Sb_{12}$ materials were diced into the desired dimensions ($A_p = 3 \times 3$ mm^2, $A_n = 1.67 \times 1.67$ mm^2, and $l_p = l_n = 1$ mm). Then, the obtained legs were treated by electroplating under a current density 100 A m^{-2} to obtain low resistance ohmic contact (Supplementary Fig. 5a). After polishing the surrounding electroplated nickel, the p- and n-type legs were assembled by a soldering process, wherein the hot side was bridged by a copper-clad plate and the cold side was welded to a direct bonding copper substrate using a tin-based solder. To obtain the temperatures of cold and hot sides, two pairs of K-type thermocouples were soldered on the cold and hot junctions of the unicouple.

Characterization
The room temperature powder X-ray diffraction (PXRD) were performed on a Rigaku, Rint 2000 instrument using Cu Kα source ($\lambda_{Cu-K\alpha} = 1.5405$ Å). The scan speed is 2°/min, and the scan step is 0.02°. The element distribution is investigated using field emission scanning electron microscopy (SEM, ZEISS SUPRA 55) equipped with energy dispersive microscopy (EDS, OXFORD Aztec XMax80). The differential scanning calorimetry (DSC) measurements were performed on Netzsch 200F3 with aluminum pans. To calculate the speed of phase transition, all samples were subjected to heating rates of 1.0, 2.0, 5.0, and 10.0 K min^{-1}. The thermal diffusivity (λ_m) was measured by laser flash method (Netzsch LFA457) under continuous argon flow. The temperature interval was set to be as small as 1 K during the phase transition region. The sample density (d) was measured by the Archimedes method. As mentioned previously, the thermal conductivity during the phase transition is calculated by $\kappa = C_{p0} \times d \times \lambda_0$, where C_{p0}, λ_0 are the heat capacity and thermal diffusivity without phase transition contribution, respectively. The total heat capacity C_p could be divided into two parts: one is the normal heat capacity (C_{p0}) from phonons and electrons without contribution from phase transition, the other is the extra energy (C_{pt}) required to transform the low-temperature trigonal phase to high-temperature cubic phase. Therefore, by subtracting the C_{pt} from C_p, we can obtain the value of C_{p0}, which is also close to the theoretical Dulong–Petit value. The Seebeck coefficient (α) and electrical resistivity (ρ) during the phase transition were measured using our previously developed system based on a thermal expansion equipment (Netzsch DIL 402 C, Supplementary Fig. 5b)[6]. Two pairs of K-type thermocouples, two Ni electrodes, and one heater were packaged into the chamber of the thermal expansion system. The ρ was measured using the standard four-probe method. The α was calculated from the slope of the ΔV vs. ΔT curve, with ΔT kept less than 3 K. The temperature dependent α and ρ were measured

under a very small temperature step (around 1 K) and a very slow heating rate (around 0.1 K/min) during phase transitions. Moreover, each temperature point was maintained for more than 20 min to ensure consistency between the sample temperature and the ambient temperature. The electrical properties before and after the phase transitions were re-measured using a commercial apparatus ZEM-3 (ULVAC) to authenticate the data (Supplementary Fig. 5c and 5d).

The cooling performance of $Cu_2Se_{1-x}S_x/Yb_{0.3}Co_4Sb_{12}$ unicouple was characterized using a self-built measurement system. As shown in Supplementary Fig. 4a, the unicouple was placed on a large Cu heat sink with heating rods inside which enables the measurement at different hot side temperatures. The testing of cooling performance is performed in a vacuumed chamber under a pressure of -10^{-3} Pa. During the measurement of ΔT with zero heat load, the DC current was provided by Agilent E3633A, the current and temperature of cold and hot sides were recorded by Keithley 2701 data acquisition system. Supplementary Fig. 4c shows the origin data measured at $T_C = 401$ K for Cu_2Se. The bule circles represent the cold side temperature on the top of p-leg. To verify the cooling performance during the phase transition, several hot side temperatures were selected to cover the temperature range of phase transitions in $Cu_2Se_{1-x}S_x$.

First-principles calculations

Ab initio molecular dynamics simulations were performed for 15 ps with a time step of 1 fs at 300 K, 350 K, 375 K, 400 K, 410 K, 425 K, and 450 K, and atomic trajectories were collected from the last 2 ps. Nine atomic configurations were picked out every 0.2 ps at each temperature based on the results of MD simulations. The band structures were calculated using density functional theory with projector-augmented-wave (PAW) pseudopotential through the Vienna ab initio Simulation Package (VASP)[51]. The generalized gradient approximation method of Perdew–Burke–Ernzerhof (PBE) and the Hubbard-type correction U_{eff} (4 eV)[52] of the Cu 3d orbital was used to describe the exchange and correlation of electrons. A plane-wave energy cutoff of 520 eV and an energy convergence criterion of 10^{-4} eV for self-consistency were adopted. The molecular dynamics simulation was conducted under constant pressure to account for the volume variation induced by temperature. As shown in Supplementary Fig. 6, the unit cell volume for the normal phases (<350 K and >425 K) gradually increases with rising temperature, demonstrating a thermal expansion effect. However, during the phase transition region, the sample exhibits a negative thermal expansion phenomenon, which is fully in line with the experimental observations[41].

Data availability

All data are available in the manuscript and in the supplementary materials.

References

1. Stanley, H. E. *Phase transitions and critical phenomena*. Clarendon Press, Oxford (1971).
2. Ma, S-K. *Modern theory of critical phenomena*. Routledge (2018).
3. Luijten, E. et al. Crossover behavior in ³He and Xe near their liquid-vapor critical point. *Phys. Rev. E* **62**, 3257 (2000).
4. Takahashi, Y. On the origin of the Curie-Weiss law of the magnetic susceptibility in itinerant electron ferromagnetism. *J. Phys. Soc. Jpn.* **55**, 3553–3573 (1986).
5. Tateiwa, N. et al. Heat-capacity anomalies at T_{sc} and T^* in the ferromagnetic superconductor UGe₂. *Phys. Rev. B* **69**, 180513 (2004).
6. Liu, H. et al. Ultrahigh thermoelectric performance by electron and phonon critical scattering in $Cu_2Se_{1-x}I_x$. *Adv. Mater.* **25**, 6607–6612 (2013).
7. Lederman, F. et al. Evidence for an order-disorder transformation in the solid electrolyte $RbAg_4I_5$. *Solid State Commun.* **19**, 147–150 (1976).
8. Avramova, I. et al. Phase transition in $Ge_{1-x}Ag_{x/2}Bi_{x/2}Te$ solid solutions and related transport phenomena. *J. Phys. Condens. Matter* **13**, 43 (2001).
9. Chen, H. et al. Thermal conductivity during phase transitions. *Adv. Mater.* **31**, 1806518 (2018).
10. Brown, D. R. et al. Relating phase transition heat capacity to thermal conductivity and effusivity in Cu2Se. *Phys. Status Solidi-Rapid Res. Lett.* **10**, 618–621 (2016).
11. Byeon, D. et al. Discovery of colossal Seebeck effect in metallic Cu_2Se. *Nat. Commun.* **10**, 1–7 (2019).
12. Bai, H. et al. An instant change of elastic lattice strain during Cu_2Se phase transition: Origin of abnormal thermoelectric properties. *Adv. Funct. Mater.* **31**, 2100431 (2021).
13. Kang, S. D. et al. Enhanced stability and thermoelectric figure-of-merit in copper selenide by lithium doping. *Mater. Today Phys.* **1**, 7–13 (2017).
14. Didisheim, J.-J. et al. Order-disorder phase transition in ZrV2D3. 6. *Solid State Commun.* **38**, 637–641 (1981).
15. Liu, H. et al. Structure-transformation-induced abnormal thermoelectric properties in semiconductor copper selenide. *Mater. Lett.* **93**, 121–124 (2013).
16. Minemura, G. et al. Electrical resistivity anomaly in the vicinity of structural phase transition of p-SnTe. *Solid State Commun.* **28**, 273–275 (1978).
17. Brown, D. R. *Enhanced thermoelectric performance at the superionic phase transitions of mixed ion-electron conducting materials*. California Institute of Technology (2015).
18. Brown, D. R. et al. Phase transition enhanced thermoelectric figure-of-merit in copper chalcogenides. *APL Mater.* **1**, 052107 (2013).
19. Ikeura, T. et al. Anomalous enhancement of seebeck coefficient in $PrIr_2Zn_{20}$. In: *Proceedings of the International Conference on Strongly Correlated Electron Systems (SCES2013))* (2014).
20. Mante, A. et al. The thermal conductivity of $BaTiO_3$ in the neighbourhood of its ferroelectric transition temperatures. *Phys. Lett. A* **24**, 139–140 (1967).
21. Kobayashi, K. et al. Resistance anomaly due to displacive phase transition in SnTe. *Solid State Commun.* **17**, 875–878 (1975).
22. Murphy, R. M. et al. Ferroelectric phase transition and the lattice thermal conductivity of $Pb_{1-x}Ge_xTe$ alloys. *Phys. Rev. B* **95**, 144302 (2017).
23. Kang, S. D. et al. Apparent critical phenomena in the superionic phase transition of $Cu_{2-x}Se$. *N. J. Phys.* **18**, 013024 (2016).
24. Ohtani, T. et al. Physical properties and phase transitions of β-$Cu_{2-x}Se$ (0.20≤x≤0.25). *J. Alloy. Compd.* **279**, 141 (1998).
25. Okamoto, K. Thermoelectric power and phase transition of Cu_2Se. *Jpn. J. Appl. Phys., Part 2* **10**, 508–508 (1971).
26. Tani, K. et al. Coupled mode of sound with soft mode in displacive-type ferroelectrics. *Phys. Lett. A* **27**, 1–2 (1968).
27. Nettleton, R. Ferroelectric phase transitions: A review of theory and experiment. Part 2—thermal conductivity. *Ferroelectrics* **1**, 87–91 (1970).
28. Takemura, M. et al. Thermal conductivity of $SrTiO_3$, $KTaO_3$ and $BaTiO_3$ near the Curie Points. *J. Phys. Soc. Jpn.* **31**, 151–154 (1971).
29. Thomas, G. et al. Thermoelectric anomaly near a critical point. *Phys. Rev. Lett.* **29**, 1321 (1972).
30. Kristoffel, N. et al. Electron-phonon interaction, microscopic mechanism and properties of ferroelectric phase transitions. *Ferroelectrics* **6**, 3–12 (1973).
31. Mahan, G. D. The Seebeck coefficient of superionic conductors. *J. Appl. Phys.* **117**, 045101 (2015).
32. Sun, S. et al. Electronic origin of the enhanced thermoelectric efficiency of Cu_2Se. *Sci. Bull.* **65**, 1888–1893 (2020).
33. Fujimoto, M. *The Physics of Structural Phase Transitions*. The Physics of Structural Phase Transitions (2005).

34. Qiu, W. J. et al. Structure family and polymorphous phase transition in the compounds with soft sublattice: Cu$_2$Se. *Ex. J. Chem. Phys.* **144**, 194502 (2016).

35. Landau, L. D. et al. Statistical physics, Part 1 (Third Edition). *Phys. Today* **34**, 74–74 (1981).

36. Bauer, R. S. et al. Electronic states of superionic conductors. *Phys. Rev. B* **13**, 3344 (1976).

37. Katayama, S. Anomalous resistivity in structural phase transition of IV–VI. *Solid State Commun.* **19**, 381–383 (1976).

38. Katayama, S. et al. Theory of anomalous resistivity associated with structural phase transitions in IV-VI compounds. *Phys. Rev. B* **22**, 336 (1980).

39. Mahan, G. *Condensed Matter in a Nutshell*. Condensed Matter in a Nutshell (2013).

40. Rao, C. N. R. Phase transitions in solids: an approach to the study of the chemistry and physics of solids / C.N.R. Rao, K.J. Rao. (1978).

41. Eikeland, E. et al. Crystal structure across the β to α phase transition in thermoelectric Cu$_{2-x}$Se. *IUCrJ* **4**, 476–485 (2017).

42. Liu, H. et al. Copper ion liquid-like thermoelectrics. *Nat. Mater.* **11**, 422 (2012).

43. Pawley, G. et al. Diatomic ferroelectrics. *Phys. Rev. Lett.* **17**, 753 (1966).

44. Chen, R. et al. Significantly optimized thermoelectric properties in high-symmetry cubic Cu$_7$PSe$_6$ compounds via entropy engineering. *J. Mater. Chem. A* **6**, 6493–6502 (2018).

45. Zhao, K. et al. Are Cu$_2$Te-based compounds excellent thermoelectric materials? *Adv. Mater.* **31**, e1903480 (2019).

46. Zhao, K. et al. Enhanced thermoelectric performance through tuning bonding energy in Cu$_2$Se$_{1-x}$S$_x$ liquid-like materials. *Chem. Mater.* **29**, 6367–6377 (2017).

47. Tang, X. et al. A comprehensive review on Bi$_2$Te$_3$-based thin films: Thermoelectrics and beyond. *Interdiscip. Mater.* **1**, 88–115 (2022).

48. Mao, J. et al. High thermoelectric cooling performance of n-type Mg$_3$Bi$_2$-based materials. *Science* **365**, 495–498 (2019).

49. Haga, H. et al. Quasicritical heat capacity at a smectic-A–hexatic-Bphase transition. *Phys. Rev. E* **56**, 1808–1818 (1997).

50. Sugimoto, N. et al. Specific heat capacity of Pb$_{1-x}$Ge$_x$Te at their structural phase transitions. *J. Phys. Soc. Jpn.* **50**, 1555–1559 (1981).

51. Kresse, G. et al. Efficient iterative schemes for ab initio total-energy calculations using a plane-wave basis set. *Phys. Rev. B* **54**, 11169 (1996).

52. Jain, A. et al. Formation enthalpies by mixing GGA and GGA+ U calculations. *Phys. Rev. B* **84**, 045115 (2011).

Acknowledgements

Author contributions

K.Z., H.C. and X.S. designed the project. Z.Y., K.Z. and P.Q. prepared the samples and carried out the transport measurements. H.C. performed the first-principles calculations. K.Z., and H.C. constructed the theoretical framework. H. W., T.D., J.L., Z.Y. and K.Z. analyzed the data. Z.Y. and K.Z. wrote the original manuscript. L.C., X.S. and K.Z. supervised the project. All the authors reviewed and edited the manuscript.

Competing interests

The authors declare no competing interests.

Additional information

Supplementary information The online version contains supplementary material available at https://doi.org/10.1038/s41467-024-45093-6.

Correspondence and requests for materials should be addressed to Kunpeng Zhao, Hongyi Chen or Xun Shi.

Peer review information : *Nature Communications* thanks Yue-Xing Chen, Zhuangfei Zhang and Nguyen Hieu for their contribution to the peer review of this work. A peer review file is available.

Reprints and permissions information is available at http://www.nature.com/reprints

Publisher's note Springer Nature remains neutral with regard to jurisdictional claims in published maps and institutional affiliations.